Analysis of colossal magnetoresistance effect in perovskite oxide heterostructures

Peng Han, Kui-juan Jin *, Hui-bin Lu, Chun-lian Hu, Guo-zhen Yang

Beijing National Laboratory for Condensed Matter Physics, Institute of Physics, Chinese Academy of Sciences, Beijing 100190, China

ABSTRACT

A systemic study of magnetoresistance (MR) in manganite perovskite oxide p–n junction is performed with experiment and theoretical calculation. The spin-dependent tunneling current is calculated with a model of double-band barrier and MR with reverse bias is explained as a result of competition between tunneling currents with different spins. The reduction of recombination rate at the interface of heterojunction with magnetic field is proposed to explain positive MR at forward bias. Furthermore, negative MR is predicted to be observed in oxide heterostructure without electron filling in $t_{2g}\downarrow$ band of manganite at the interface region with both forward and reverse bias.

© 2011 Elsevier B.V. All rights reserved.

1. Introduction

The magnetoresistance (MR) in the low-dimensional system of the manganite oxide including films [1,2], p–n junctions [3–11], magnetic tunnel junctions [12,13], and superlattices [14,15] has attracted great attention since the colossal magnetoresistance (CMR) effect has been observed in $La_{0.67}Ca_{0.33}MnO_3$ film in the last decade [16]. In these oxide microstructures, huge positive and negative MR rates have been measured with both forward (a positive voltage applied to the p-region with respect to the n-region) and reverse (a positive voltage applied to the n-region with respect to the p-region) bias [3–11], respectively. Comparing to the huge progress in the experiment, the theoretical study on the mechanism of CMR is more complicated due to the interplay of spin, charge, orbital, and the competition of this closely related energy scaled. In the early stage, the double-exchange (DE) model was proposed by Zener to explain the mechanism of MR [17,18]. Furthermore, a strong electron–phonon interaction arising from the Jahn–Teller distortion has been supplied to the DE model [19]. In contrast to the DE model, an alternative idea was proposed on the fact that the holes are located in the oxygen orbital of the charge-transfer materials [20–24]. In that model, the doped holes mainly reside on the oxygen orbital and interact with Mn ions by a d–p exchange interaction. Due to the negative integral of the d–p exchange, these holes are linked antiferromagnetically with the spins of the adjacent Mn ions [17,20–24]. By applying a magnetic field, the movement of the holes would be improved with all the Mn spins are aligned. In addition to the complicated origin of CMR

in manganite materials, the mechanism of the novel MR behaviors in the manganite oxide heterostructures remains controversy. To explore the physical mechanism of positive MR in the manganite heterojunction at reverse bias, a phenomenological model has been proposed [25] based on the band structures of hole-doped manganite material at the interface region of the heterojunction. With this model, the positive MR properties in various manganite heterostructure systems [25–27] have been explained. However, a self-consistent calculation of this phenomenological model and the comparison between the calculated results with experimental data are still lacking. In addition, neither experimental nor theoretical study for heterostructures at forward bias has been reported yet.

In this Letter, we report a systemic study of the spin-polarized transport process in $La_{0.9}Sr_{0.1}MnO_3/SrNb_{0.01}Ti_{0.99}O_3$ (LSMO/SNTO) p–n junction based on both experimental and theoretical results. The theoretical spin-polarized currents are calculated with a model of double-band barrier for tunneling and with spin-dependent drift-diffusion model. Within our phenomenological model, the spin-dependent drift-diffusion current with forward bias is a function of the recombination rate between the spin-polarized electrons and holes at the interface of the heterojunction. At reverse bias, the spin-polarized tunneling current is determined by the bias-dependent band structure, filling of t_{2g} spin-down ($t_{2g}\downarrow$) band, and the alignment of e_g^1 spin-up ($e_g^1\uparrow$) band with $t_{2g}\downarrow$ and e_g^2 spin-up ($e_g^2\uparrow$) bands in the p-LSMO region. Based on the calculated spin-dependent currents, the MR rate with a certain spin-polarization rate P is defined as $MR = (R(P) - R(0))/R(0) = J(0)/J(P) - 1$, where $R(P)$ and $J(P)$ are spin-dependent resistance and current density, respectively. As indicated in this definition, a positive MR will be obtained when the current density decreases with the increase of spin-polarization rate. The positive

* Corresponding author. Tel.: +86 10 82648099.
E-mail address: kjjin@aphy.iphy.ac.cn (K.-j. Jin).

MR effect observed in the LSMO/SNTO heterojunction with forward bias is concluded to be the reduction of recombination rate between electrons in the $t_{2g}\downarrow$ band and holes in the $e_g^1\uparrow$ band in the p-LSMO region with the increase of applied magnetic field. With the reverse bias, the theoretical MR curves are obtained by computing the spin-dependent tunneling currents from $e_g^1\uparrow$ to $t_{2g}\downarrow$ band and from $e_g^1\uparrow$ to $e_g^2\uparrow$ band with the model of double-band barrier for tunneling. Comparing with the calculated and the measured MR curves, the positive MR at reverse bias can be explained with the variation of tunneling rates for spin up and down electrons and the strong scattering between electrons with different spins in the $t_{2g}\downarrow$ band of manganite at the interface region. In addition, the negative MR is predicted to be measured in the heterojunctions without electron filling in the $t_{2g}\downarrow$ band of manganite material at the interface region with both forward and reverse bias, respectively.

2. Experiment

The experimental setup, the measurement method, and the data analysis have been given in details in Refs. [6,7,9,10,25,26]. Here, we only outline them briefly. The LSMO/SNTO heterojunction was fabricated by using the laser molecular-beam epitaxy (laser MBE). The 0.1 Sr-doped LaMnO$_3$ with thickness of 400 nm was deposited directly on the 0.01 Nb-doped SrTiO$_3$ at the substrate temperature as 630 °C with the oxygen pressure as 2×10^{-3} Pa. With the laser wavelength of 308 nm, repetition rate of 2 Hz, and duration as 20 ns, the growth rate of LSMO was about 1.3 nm/min. The XRD θ–2θ scan curve and the cross-section high-resolution transmission electron microscopic (HRTEM) image show that good interface between LSMO and SNTO was obtained.

The temperature-dependent resistance measurements were performed on the LSMO and SNTO films by using the in-plane currents and the four-point geometry method. The measured temperature-dependent resistance curves, which are given in Ref. [25], indicated a negative CMR property of the LSMO film and the semiconducting transport characteristics of both LSMO and SNTO films in the temperature range from 75 to 345 K. The I–V characteristics of the LSMO/SNTO heterojunction without the applied magnetic field were measured by using a pulse-modulated current source with the step of 0.01 mA. The I–V behaviors of the LSMO/SNTO heterojunction under the magnetic field were measured by using the superconducting quantum interference device (SQUID) at the temperature 190 and 255 K, respectively. The magnetic field was applied perpendicular to the heterojunction interface and parallel to the current in the range from 5 to 1000 Oe. The measured MR curves as the functions of the positive and negative bias voltages are plotted in Figs. 1(a) and 2(a), respectively. As shown in these figures, the magnetic resistance MR $= (R_H - R_0)/R_0$ increases with the increased applied magnetic field, which shows the positive MR phenomenon.

3. Theoretical model

In the bulk hole-doped LSMO, three of the Mn-3d electrons form the lower energy t_{2g} band and the remaining two electrons occupy the higher energy e_g band in the cubic crystal field. Due to the Jahn–Teller distortion, the e_g band splits further to the e_g^1 and e_g^2 bands. Furthermore, the spin degeneracy is removed into the magnetic states by Hund's rule coupling. Based on the hypothesis of weak Hund's rule coupling [13,25], the $t_{2g}\downarrow$ band is energetically higher than the $e_g^1\uparrow$ band and lower than the $e_g^2\uparrow$ band. When the p-LSMO film is deposited on the n-SNTO film, the electrons in the n-SNTO film and holes in the p-LSMO film will diffuse into the p-LSMO and n-SNTO regions, respectively. Due to the band
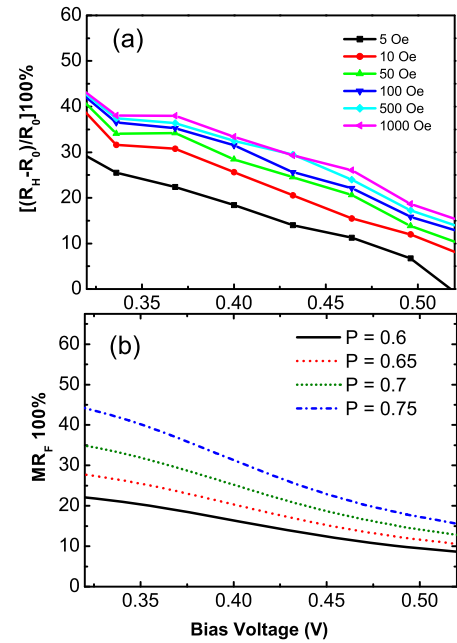

Fig. 1. (Color online.) The measured (a) and calculated (b) MR curves with various applied magnetic fields (or spin polarization rates) under forward bias voltage at $T = 255$ K.
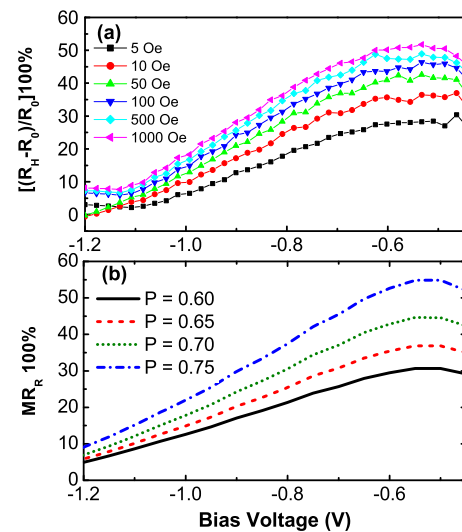

Fig. 2. (Color online.) The measured (a) and calculated (b) MR curves with various applied magnetic fields (or spin polarization rates) under reverse bias voltage at $T = 190$ K.

structure of the p-LSMO, the $t_{2g}\downarrow$ band will be partially filled after the filling of the $e_g^1\uparrow$ band at the interface region of the p-LSMO. Then the build-in electric field will be built up to balance the effect of drift and diffusion, and the p-LSMO/n-SNTO heterojunction is formed.

Based on the study of spin-independent transport process in the perovskite heterojunction [28], Poisson equation and the spin-dependent drift-diffusion equations are employed to describe the behavior of electrostatic potential $\phi(x)$, the spin polarized electrons $n_\sigma(x)$ and holes $p_\sigma(x)$ ($\sigma = \uparrow, \downarrow$ for spin up and down state, respectively) with a certain value of P. Here, $P = (N_\uparrow - N_\downarrow)/(N_\uparrow + N_\downarrow)$ is defined as spin polarization rate with $N_\uparrow$ and $N_\downarrow$ denoting the density of states with majority and minority spins, respectively. Without considering the flipping of spin state during

the transport process, the spin-dependent continuity equations are written as,

$$\frac{d\,J_{n,\sigma}(x, P)}{dx} = qR_\sigma(x),$$

$$\frac{d\,J_{p,\sigma}(x, P)}{dx} = -qR_\sigma(x), \tag{1}$$

where $R_\sigma(x)$ denotes the spin-dependent recombination rate of the Shockley–Read–Hall recombination processes [29–31], and q is the electron charge. The spin-dependent drift-diffusion current is

$$J_{n,\sigma}(x, P) = -\mu_n\left[qn_\sigma(x)\frac{d\phi(x)}{dx} + k_BT\frac{dn_\sigma(x)}{dx}\right],$$

$$J_{p,\sigma}(x, P) = -\mu_p\left[qp_\sigma(x)\frac{d\phi(x)}{dx} - k_BT\frac{dp_\sigma(x)}{dx}\right], \tag{2}$$

where k_B denotes the Boltzmann's constant, T is the temperature, μ_n and μ_p represent the mobilities of electrons and holes, respectively. Due to the strong scattering between carriers with different spins, we only consider the recombination process between carriers with the same spin orientation. Thus the spin-dependent recombination rate is written as,

$$R_\sigma(x) = \frac{p_\sigma(x)n_\sigma(x) - n_{i,\sigma}^2}{\tau_n[p_\sigma(x) + n_{i,\sigma}] + \tau_p[n_\sigma(x) + n_{i,\sigma}]}, \tag{3}$$

where $n_{i,\sigma}$ denotes the spin-polarized intrinsic carrier concentration, τ_n and τ_p describe the lifetime for electron and hole, respectively.

In the LSMO/SNTO heterojunction, the band structure of LSMO is hypothesized as weak Hund's rule coupling. With this hypothesis, $t_{2g}\downarrow$ band is energetically lower than $e_g^2\uparrow$ band and the former is partially filled at the interface of the heterojunction [13,25]. Thus $t_{2g}\downarrow$ and $e_g^1\uparrow$ band are the conduction and valence band of p-LSMO, respectively. The spin-polarized electron and hole concentrations at $x = 0$ are $p_\uparrow(0) = \frac{1+P}{2}N_a$, $p_\downarrow(0) = \frac{1-P}{2}N_a$, $n_\uparrow(0) = \frac{1-P}{2}n_i^2(0)/N_a$, and $n_\downarrow(0) = \frac{1+P}{2}n_i^2(0)/N_a$, respectively. $n_i(0)$ and N_a denote the concentrations of non-spin polarized intrinsic carrier and the ionized acceptor at the p-region, respectively. For the nonmagnetic SNTO, the boundary conditions of carriers are $p_\uparrow(L) = p_\downarrow(L) = \frac{1}{2}n_i^2(L)/N_d$ and $n_\uparrow(L) = n_\downarrow(L) = \frac{1}{2}N_d$, respectively. Here, $n_i(L)$ and N_d denote the concentrations of intrinsic carrier and the ionized donor at the n-region, respectively. The electrostatic potentials at two sides of the heterojunction are $\phi(0) = 0$ and $\phi(L) = V_d - V_{bias}$ with V_d is the build-in potential. With these boundary conditions, the total forward current $J_F(P) = \sum_{\sigma=\uparrow,\downarrow} J_{n,\sigma}(x, P) + J_{p,\sigma}(x, P)$ is obtained self-consistently. The calculated band structures of LSMO/SNTO heterojunction with $+0.5$ V and -1.0 V bias are plotted in Figs. 3 and 4, respectively.

In the case of reverse bias, the spin-dependent interband and trap assisted tunneling processes are analyzed with the hypothesis of weak Hund's rule coupling and the free electron model is introduced to calculate the electron tunneling current. As plotted in Fig. 4, the potential barrier for tunneling between $e_g^1\uparrow$ band into $t_{2g}\downarrow$ (or $e_g^2\uparrow$) band $V_{t_{2g}}(x)$ (or $V_{e_g^2}(x)$) is determined by the top of $e_g^1\uparrow$ band and the bottom of $t_{2g}\downarrow$ (or $e_g^2\uparrow$) band, respectively. Thus, a double-band barrier for tunneling is constructed. With this double-band barrier, the spin up and down electrons tunnel through various potential barriers. Therefore, the tunneling rate for spin down electrons is greater than that for spin up ones.

The wave functions of electrons with kinetic energy E, $\psi_{E,\uparrow\to\uparrow}(x)$ (or $\psi_{E,\uparrow\to\downarrow}(x)$) satisfy the stationary effective-mass
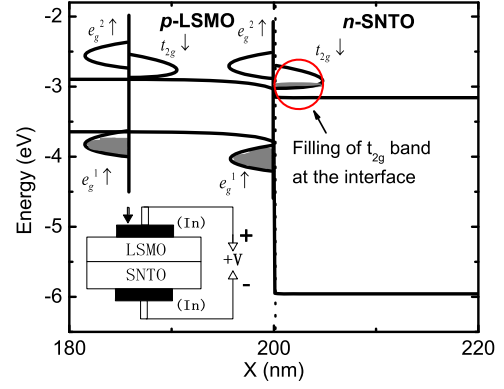

Fig. 3. (Color online.) The band–energy profile of the La$_{0.9}$Sr$_{0.1}$MnO$_3$/SrNb$_{0.01}$Ti$_{0.99}$O$_3$ heterojunction with $+0.5$ V bias applied across the entire system.
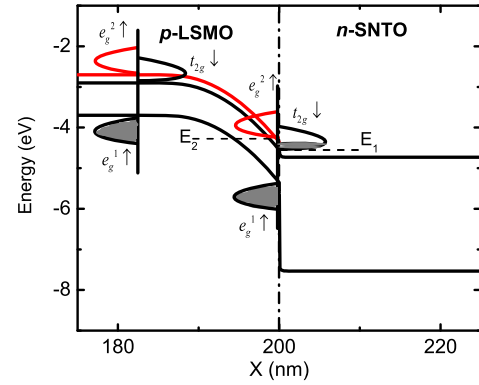
Fig. 4. (Color online.) The band–energy profile of the La$_{0.9}$Sr$_{0.1}$MnO$_3$/SrNb$_{0.01}$Ti$_{0.99}$O$_3$ heterojunction with -1.0 V bias applied across the entire system.

Schrödinger equation with the double-band barrier as follows,

$$-\frac{\hbar^2}{2m^*}\frac{d^2\psi_{E,\uparrow\to\uparrow}(x)}{dx^2} - qV_{e_g^2}(x)\psi_{E,\uparrow\to\uparrow}(x) = E\psi_{E,\uparrow\to\uparrow}(x),$$

$$-\frac{\hbar^2}{2m^*}\frac{d^2\psi_{E,\uparrow\to\downarrow}(x)}{dx^2} - qV_{t_{2g}}(x)\psi_{E,\uparrow\to\downarrow}(x) = E\psi_{E,\uparrow\to\downarrow}(x), \tag{4}$$

where $\hbar$ represents the reduced Planck constant and m^* is the effective mass of electron. We should point out here that the potential barrier for tunneling is assumed to be constant during the tunneling process. Or in other words, the variation of the distribution of charge density caused by tunneling process is ignored in the calculation. This assumption is a reasonable approximation for treating the tunneling process in p–n junction. Thus, the wave functions are time independent in this work. Based on the free electron model of the conduction electrons [32,33], the solutions of Eq. (4) are plane waves in the intervals $0 \leqslant x < a$ and $b < x \leqslant L$, where a and b are the boundaries of tunneling barrier, respectively. The wave functions are written as,

$$\psi_{E,\uparrow\to\sigma}(x) = e^{i\sqrt{2m^*E}x/\hbar} + r_{\uparrow\to\sigma}(E)e^{-i\sqrt{2m^*E}x/\hbar} \quad (x < a),$$

$$\psi_{E,\uparrow\to\sigma}(x) = t_{\uparrow\to\sigma}(E)e^{i\sqrt{2m^*E}x/\hbar} \quad (x > b), \tag{5}$$

where $r_{\uparrow\to\sigma}(E)$ and $t_{\uparrow\to\sigma}(E)$ denote the reflection and transmission amplitudes, respectively. Solving Eqs. (4) and (5) with the finite difference discrete formulation and the open boundary conditions [33], the spin-dependent tunneling rate $T_{\uparrow\to\sigma}(E) = \frac{\hbar}{\sqrt{2m^*E}}\mathrm{Im}[\psi_{E,\uparrow\to\sigma}^*(x)\frac{d}{dx}\psi_{E,\uparrow\to\sigma}(x)]$ is obtained with "Im" denoting the imaginary part of a complex number. Because the wave functions are treated as time independent in our work, the expres-

sion of $\text{Im}[\psi^*_{E,\uparrow\to\sigma}(x)\frac{d}{dx}\psi_{E,\uparrow\to\sigma}(x)]$ is spatial independent, and the tunneling rate can be written as $T_{\uparrow\to\sigma}(E)$.

By solving the spin-dependent tunneling Hamiltonian, the direct tunneling current densities $J_{DT\uparrow\to\uparrow}(P)$ and $J_{DT\uparrow\to\downarrow}(P)$ are written as

$$J_{DT\uparrow\to\uparrow}(P) = q\frac{1+P}{2}\left[\int_{E_{Fn}}^{E_1} N(E)f(E)T_{\uparrow\to\uparrow}(E)\,dE\right.$$
$$\left.+\int_{E_2}^{E_{vp}} N(E)f(E)T_{\uparrow\to\uparrow}(E)\,dE\right],$$

$$J_{DT\uparrow\to\downarrow}(P) = q\frac{1-P}{2}\int_{E_{Fn}}^{E_{vp}} N(E)f(E)T_{\uparrow\to\downarrow}(E)\,dE, \tag{6}$$

where E_{Fn} is the Fermi level in the homogeneous region of the n side and E_{vp} denotes the top of valence band in the homogeneous region of p side, respectively. E_1 and E_2 are the bottom of $t_{2g}\downarrow$ and $e_g^1\uparrow$ band at the interface of the heterojunction as indicated in Fig. 4, respectively. $N(E)$ denotes the density of state in the $e_g^1\uparrow$ band and $f(E)$ represents the Fermi distribution function.

Besides the direct tunneling current, the spin-dependent trap assisted tunneling current caused by the states induced by the oxygen vacancies is also considered in the spin polarized transport process. The spin-dependent trap assisted tunneling currents are written as [28,34]

$$J_{TAT\uparrow\to\uparrow}(P) = q\frac{1+P}{2}N_t\sigma_t\left[\int_{E_{Fn}}^{E_1} \frac{N(E)f(E)T_1(E)T_{2,\uparrow\to\uparrow}(E)}{T_1(E)+T_{2,\uparrow\to\uparrow}(E)}\,dE\right.$$
$$\left.+\int_{E_2}^{E_{vp}} \frac{N(E)f(E)T_1(E)T_{2,\uparrow\to\uparrow}(E)}{T_1(E)+T_{2,\uparrow\to\uparrow}(E)}\,dE\right],$$

$$J_{TAT\uparrow\to\downarrow}(P) = q\frac{1-P}{2}N_t\sigma_t\int_{E_{Fn}}^{E_{vp}} \frac{N(E)f(E)T_1(E)T_{2,\uparrow\to\downarrow}(E)}{T_1(E)+T_{2,\uparrow\to\downarrow}(E)}\,dE, \tag{7}$$

where N_t represents the density of traps and σ_t denotes the effective capture cross section. The value of $N_t\sigma_t$ is estimated as 0.15 in the calculation [28]. $T_1(E)$ and $T_{2,\uparrow\to\downarrow}(E)$ (or $T_{2,\uparrow\to\uparrow}(E)$) are the tunneling rate of electrons tunnel from $e_g^1\uparrow$ band into traps and from traps into the $t_{2g}\downarrow$ (or $e_g^2\uparrow$) band, respectively. Combining the direct and trap assisted tunneling current, the total reverse current $J_R(P)$ is obtained.

4. Results and discussion

With above formulas, the spin-dependent I–V characteristics are calculated self-consistently over a wide range of bias voltages. The concentrations of the acceptor and the donor are $N_a = 8.0 \times 10^{19}$ cm^{-3} and $N_d = 5.0 \times 10^{20}$ cm^{-3} in our calculation, respectively. It should be pointed out here that the hole concentration used in the present work is much less than the reported value. The low measured carrier concentration may come from the inhomogeneity of the LSMO film. The other necessary parameters are taken the same values as those used in our previous works [25,28]. In addition, the band gap between $e_g^1\uparrow$ and $t_{2g}\downarrow$ is set as 0.8 eV, while that for $e_g^1\uparrow$ and $e_g^2\uparrow$ is set as 0.9 eV [35]. To analyze the MR rate with a given spin polarization rate P, we define
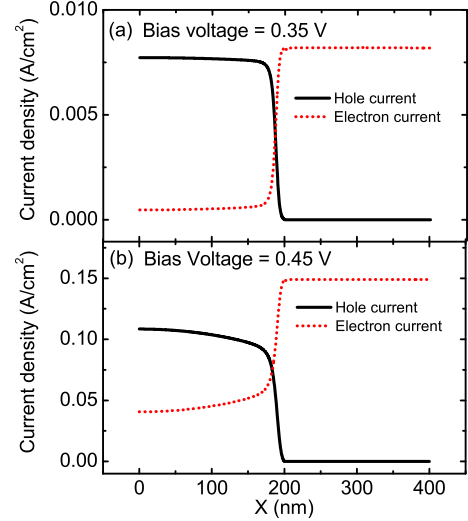

Fig. 5. (Color online.) The calculated hole current density (solid curve) and electron current density (dotted curve) with 0.35 V bias (a) and 0.45 V bias (b).

the forward MR rate as $\text{MR}_F(P) = [R_F(P) - R_F(0)]/R_F(0) = J_F(0)/J_F(P) - 1$ and reverse MR rate as $\text{MR}_R(P) = [R_R(P) - R_R(0)]/R_R(0) = J_R(0)/J_R(P) - 1$, respectively. Here, $R_{F(R)}(P)$ is the resistance of LSMO/SNTO heterojunction at forward (reverse) bias with spin polarization rate P under the applied magnetic field and $R_{F(R)}(0)$ is the one without magnetic field, respectively. The values of $\text{MR}_F(P)$ and $\text{MR}_R(P)$ are calculated by solving Eqs. (1)–(7), respectively.

The measured and the calculated MR curves with forward bias on the heterojunction at $T = 255$ K are given in Figs. 1(a) and 1(b), respectively. Comparing with the experimental data, the theoretical curves have the same trend with the increase of bias voltage and the spin polarization rate. As shown in these figures, the value of MR curves increases with the increase of applied magnetic field (or the spin polarization rate) as the behavior of positive MR and decreases with the increase of bias voltage. These properties can be explained as follows. Based on the hypothesis of weak Hund's rule coupling, the $e_g^1\uparrow$ band and the $t_{2g}\downarrow$ band are the valence and conduction band of the p-LSMO, respectively. The concentrations of spin up hole and spin down electron increase with the applied magnetic field. Due to the strong scattering between carriers with different spins, only the recombination process between carriers with the same spins is considered. Therefore, the recombination current decreases with the increase of magnetic field and the positive MR is obtained in the LSMO/SNTO heterojunction. To understand the decrease of MR value with the increase of bias voltage, the comparison between electron and hole current with bias voltage as 0.35 and 0.45 V with $P = 0$ is plotted in Figs. 5(a) and 5(b), respectively. As indicated in these figures, the effect of recombination on the transport current decreases with the increase of bias voltage, and therefore the effect of spin polarization on the transport of carriers decreases.

Based on this understanding, the strong scattering between electrons with down spins in $t_{2g}\downarrow$ band and holes with up spins in $e_g^1\uparrow$ band at the interface region is crucial for the positive MR with forward bias. Therefore, the positive MR should not be observed in the heterojunction without electron filling in the $t_{2g}\downarrow$ band of manganite material at the interface region. In this case, the heterojunction will present the negative CMR property of the manganite material at forward bias.

In the case of reverse bias, the comparison between the experimental and calculated MR curves with various applied magnetic fields (or the spin polarization rates) at $T = 190$ K are illustrated

in Figs. 2(a) and 2(b), respectively. The experimental data are obtained from the previous work of our group [25]. As indicated in these figures, the MR value increases with the increase of reverse bias and obtains its peak value at about -0.5 V, and then decreases with the further increase of reverse bias. In addition, the MR value increases with the applied magnetic field as the behavior of positive MR. The properties of MR with reverse bias can be understood from the following two aspects. Firstly, as indicated in the model of double-band barrier, the tunneling rate for spin down electrons is greater than that for spin up ones. With the increase of applied magnetic field, the concentration of spin up electrons increases and that for spin down ones decreases in the $e_g^1\uparrow$ band of the LSMO region. Thus the total tunneling current density decreases with the increase of applied magnetic field. Besides the variation of barrier width for tunneling, the strong scattering between electrons with different spins in the $t_{2g}\downarrow$ band at the interface region also plays a very important role for the positive MR in the LSMO/SNTO heterojunction. At very small reverse bias, the energy of E_{vp} is lower than that of E_1 and electrons with both spin up and down states can transport from the $e_g^1\uparrow$ band of p side into the conduction band of n side by direct and trap assisted tunneling processes without contributions to the MR effect. With the increase of revers bias, the energy of E_1 and E_2 decreases and electrons in the $e_g^1\uparrow$ band of p side not only tunnel into the conduction band of n side but also tunnel into the conduction band of the space charge region in p side, as shown in Fig. 4. In the condition of $E_1 < E_{vp} < E_2$, electrons in the $e_g^1\uparrow$ band of p side can tunnel into the $t_{2g}\downarrow$ band in the space charge region and the conduction band of n side. With the increase of applied magnetic field, the concentrations of spin up and down electrons increase in the $e_g^1\uparrow$ and $t_{2g}\downarrow$ band, respectively. The tunneling current decreases due to the increase of scattering between electrons with two spin states in the $t_{2g}\downarrow$ band. Thus, the value of MR rate increases and the property of positive MR is obtained. With the further increase of bias, E_{vp} is higher than E_2 and electrons in the $e_g^1\uparrow$ band of p side can tunnel into the $e_g^2\uparrow$ band in the space charge region. Therefore, the majority channel of spin up electrons is available for the transport and the MR value decreases with the further increase of reverse bias voltage.

As indicated in the spin-dependent tunneling process in the LSMO/SNTO heterojunction, the electron filling in the $t_{2g}\downarrow$ band of LSMO material at the interface region also plays a very important role for the positive MR at reverse bias. Without the electron filling in the $t_{2g}\downarrow$ band, electrons with both spins can tunnel into the $t_{2g}\downarrow$ band and $e_g^2\uparrow$ band without strong scattering. Thus, the negative MR phenomenon caused by the negative CMR property of LSMO material will be measured in the heterojunction.

5. Summary

In summary, the spin polarization transport processes of the p-manganite/n-titanate heterostructure have been systemically studied in this work. The spin-polarized current densities at forward and reverse bias are calculated self-consistently based on the spin-dependent drift-diffusion model and the direct and trap assisted tunneling theory with the double-band barrier model, respectively. The agreement between the experimental data and the theoretical results reveals that the decrease of recombination rate of electrons in the $t_{2g}\downarrow$ band and holes in the $e_g^1\uparrow$ band with the increase of applied magnetic field is the physical mechanism of positive MR

in LSMO/SNTO heterojunction with forward bias. Based on the calculation with the model of double-band barrier for tunneling, the characteristics of MR curves at reverse bias are concluded to be the results of the competition between tunneling currents from $e_g^1\uparrow$ to $t_{2g}\downarrow$ band and from $e_g^1\uparrow$ to $e_g^2\uparrow$ band with the increase of bias voltage and applied magnetic field. In addition, based on our calculation, negative MR effect is predicted to be measured in the perovskite oxide heterojunctions without electron filling in the $t_{2g}\downarrow$ band at the interface region of the manganite material.

References

[1] J. O' Donnell, M. Onellion, M.S. Rzchowski, J.N. Eckstein, I. Bozovic, Phys. Rev. B 54 (1996) 8641.
[2] W. Prellier, Ph. Lecoeur, B. Mercey, J. Phys.: Condens. Matter 13 (2001) 915.
[3] H. Tanaka, J. Zhang, K. Kawai, Phys. Rev. Lett. 88 (2002) 027204.
[4] J. Zhang, H. Tanaka, K. Kawai, Appl. Phys. Lett. 80 (2002) 4378.
[5] C. Mitra, G. Köbernik, K. Dörr, K.H. Müller, L. Schultz, P. Raychaudhuri, R. Pinto, E. Wieser, J. Appl. Phys. 91 (2002) 7715.
[6] H.B. Lu, G.Z. Yang, Z.H. Chen, S.Y. Dai, Y.L. Zhou, K.J. Jin, B.L. Cheng, M. He, L.F. Liu, H.Z. Guo, Y.Y. Fei, W.F. Xiang, L. Yan, Appl. Phys. Lett. 84 (2004) 5007.
[7] H.B. Lu, S.Y. Dai, Z.H. Chen, Y.L. Zhou, B.L. Cheng, K.J. Jin, L.F. Liu, G.Z. Yang, X.L. Ma, Appl. Phys. Lett. 86 (2005) 032502.
[8] T.F. Zhou, G. Li, N.L. Wang, B.M. Wang, X.G. Li, Y. Chen, Appl. Phys. Lett. 88 (2006) 232508.
[9] K.J. Jin, H.B. Lu, K. Zhao, C. Ge, M. He, G.Z. Yang, Adv. Mater. 21 (2009) 4636.
[10] C. Ge, K.J. Jin, H.B. Lu, C. Wang, Mod. Phys. Lett. B 23 (2009) 1129.
[11] T. Susaki, N. Nakagawa, H.Y. Hwang, Phys. Rev. B 75 (2007) 104409.
[12] J.M. De Teresa, A. Barthelemy, A. Fert, J.P. Contour, R. Lyonnet, F. Montaigne, P. Seneor, A. Vaures, Phys. Rev. Lett. 82 (1999) 4288.
[13] C. Mitra, P. Raychaudhuri, K. Dörr, K.H. Müller, L. Schultz, P.M. Oppeneer, S. Wirth, Phys. Rev. Lett. 90 (2003) 017202.
[14] G.Q. Gong, A. Gupta, G. Xiao, P. Lecoeur, T.R. McGuire, Phys. Rev. B 54 (1996) R3742.
[15] M.P. Singh, W. Prellier, C. Simon, B. Raveau, Appl. Phys. Lett. 87 (2005) 022505.
[16] S. Jin, T.H. Tiefel, M. McCormack, R.A. Fastnact, R. Ramesh, L.H. Chen, Science 264 (1994) 413.
[17] E. Dagotto, T. Hotta, A. Moreo, Phys. Rep. 344 (2001) 1.
[18] C. Zener, Phys. Rev. 82 (1951) 403.
[19] A.J. Millis, B.L. Shraiman, R. Mueller, Phys. Rev. Lett. 77 (1996) 175.
[20] M.A. Subramanian, B.H. Toby, A.P. Ramirez, W.J. Marshall, A.W. Sleight, G.H. Kwei, Science 273 (1996) 81.
[21] G.M. Zhao, Phys. Rev. B 62 (2000) 11639.
[22] G.M. Zhao, Y.S. Wang, D.J. Kang, W. Prellier, M. Rajeswari, H. Keller, T. Venkatesan, C.W. Chu, R.L. Greene, Phys. Rev. B 62 (2000) R11949.
[23] A. Nucara, A. Perucchi, P. Calvani, T. Aselage, D. Emin, Phys. Rev. B 68 (2003) 174432.
[24] A.S. Alexandrov, A.M. Bratkovsky, V.V. Kabanov, Phys. Rev. Lett. 96 (2006) 117003.
[25] K.J. Jin, H.B. Lu, Q.L. Zhou, K. Zhao, B.L. Cheng, Z.H. Chen, Y.L. Zhou, G.Z. Yang, Phys. Rev. B 71 (2005) 184428.
[26] K.J. Jin, H.B. Lu, Q.L. Zhou, K. Zhao, G.Z. Yang, J. Magn. Magn. Mater. 303 (2006) 329.
[27] C.M. Xiong, Y.G. Zhao, B.T. Xie, P.L. Lang, K.J. Jin, Appl. Phys. Lett. 88 (2006) 193507.
[28] P. Han, K.J. Jin, H.B. Lu, Q.L. Zhou, Y.L. Zhou, G.Z. Yang, Appl. Phys. Lett. 91 (2007) 182102.
[29] K. Horio, H. Yanai, IEEE Trans. Electron Devices 37 (1990) 1093.
[30] K. Yang, J.R. East, G.I. Haddad, Solid-State Electron. 36 (1993) 321.
[31] P. Han, Y. Zhou, K.-J. Jin, X. Wang, Z. Ma, S.F. Ren, A.G. Mal'shukov, K.A. Chao, J. Appl. Phys. 99 (2006) 074504.
[32] J.C. Slonczewski, Phys. Rev. B 39 (1989) 6995.
[33] O. Pinaud, J. Appl. Phys. 92 (2002) 1987.
[34] E. Suzuki, D.K. Schroder, Y. Hayashi, J. Appl. Phys. 60 (1986) 3616.
[35] R. Rauer, M. Rübhausen, K. Dörr, Phys. Rev. B 73 (2006) 092402.